Uni-axial reinforced dielectric elastomer actuators with embedded 3D printed fibers

OPEN ACCESS
IOP Publishing
Smart Materials and Structures
Smart Mater. Struct. **32** (2023) 125011 (13pp)
https://doi.org/10.1088/1361-665X/ad0447

Uni-axial reinforced dielectric elastomer actuators with embedded 3D printed fibers

Stefania Konstantinidi[1,*], Thomas Martinez[1], Biranche Tandon[2], Yoan Civet[1] and Yves Perriard[1]

[1] Ecole Polytechnique Fédérale de Lausanne (EPFL), Integrated Actuators Laboratory (LAI), Neuchâtel, Switzerland
[2] Ecole Polytechnique Fédérale de Lausanne (EPFL), Microsystems Laboratory (LMIS1), Lausanne, Switzerland

E-mail: stefania.konstantinidi@epfl.ch

Received 24 July 2023, revised 29 August 2023
Accepted for publication 17 October 2023
Published 3 November 2023

Abstract

Dielectric elastomer actuators (DEAs) can be described as compliant capacitors formed by a dielectric elastomer film sandwiched between two electrodes. An applied voltage results in a compressive Maxwell stress, a thickness reduction and thus an expansion in the other dimensions. In order to favor large uni-axial deformations, it is predicted that DEAs ought to be constrained in the other direction. This can be achieved by reinforcing the DEA with unidirectional fibers. In this paper, the behavior of uni-axial fiber-reinforced DEAs is established and the proposed model innovates by taking into consideration the fiber properties such as their Young's modulus and dimensions, and is characterized by transversely isotropic models. A novel fabrication process is then presented for reinforced DEAs by using 3D printed fibers with four different materials, namely Nylon, PETG, ABS and PLA, and different coverages of fibers are considered. Fiber reinforcement is shown to increase uni-axial strain up to 75% in the manufactured DEAs when compared to traditional DEAs. This behavior corresponds to the one predicted by the proposed model.

Keywords: DEAs, fiber reinforcement, soft actuators, smart materials

(Some figures may appear in colour only in the online journal)

1. Introduction

Artificial muscles consist of soft actuators executing a movement similar to the one of natural biological muscles. Existing technologies are currently studied and used in the domain of robotics and prosthesis, and their operation includes pneumatic [1], thermal [2] and electrical mechanisms [3] among others.

Inspired by biological tissue and muscles, fiber-reinforced artificial muscles have been developed in recent years by embedding fibers in the actuator [4, 5]. Fiber reinforcement allows to keep the soft properties of the actuator while guiding and/or the constraint movement in specific directions. Fiber reinforced composites and biological tissues are anisotropic in nature due to the microstructural arrangement, and thus show direction dependant properties. A common fiber reinforced artificial muscle is the traditional McKibben actuator [6], consisting of a pneumatic chamber inside a braided mesh. When the inner chamber is under pressure, it will expand

* Author to whom any correspondence should be addressed.

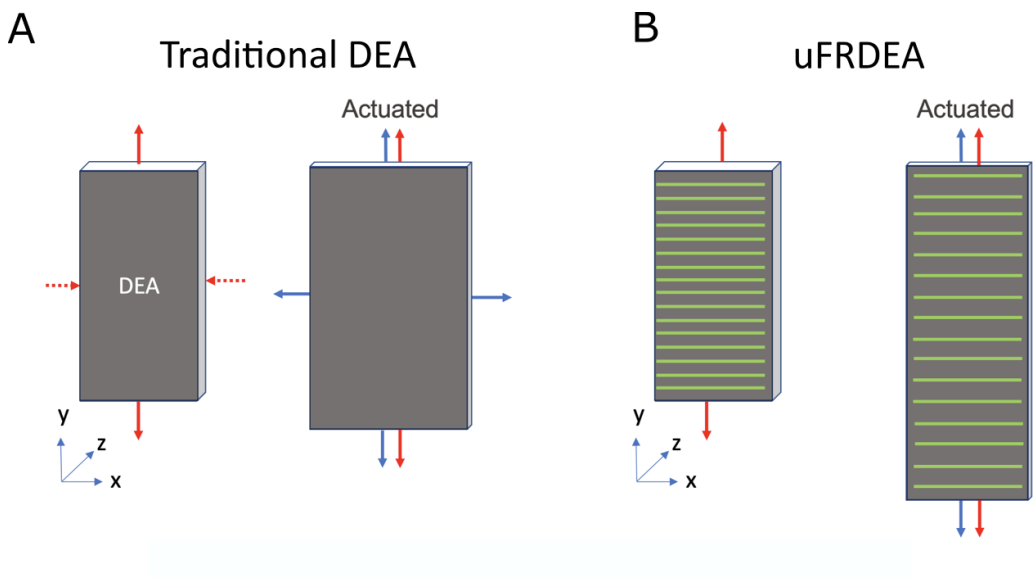

Figure 1. DEA principle of operation. The application of voltage induces a compressive Maxwell stress, causing a decrease in thickness and expansion in perpendicular directions. (A) DEA submitted to uni-axial external forces (red arrows) and its corresponding actuated state (blue arrows). The strain in the the direction of the load (*y*-axis) is low, whereas the strain in the perpendicular direction (*x*-axis) is large. (B) uFRDEA submitted to the same uni-axial external forces, at rest and when a voltage is applied. The strain on the *x* axis is constrained and the strain in the *y* axis is enhanced.

and the mesh will translate the radial expansion into a linear contraction.

Dielectric elastomer actuators (DEAs) are a type of electroactive polymers (EAPs) [7], which are materials capable of inducing mechanical displacement under electrical stimulation. Thus, DEAs deform under an applied electric field, making them promising for a wide range of applications including soft robots and haptic interfaces. DEAs can be described as compliant capacitors; a dielectric elastomer film is coated by two compliant electrodes. An applied voltage results in a compressive Maxwell stress, leading to a thickness reduction and a consequent expansion in the other dimensions, as illustrated in figure 1(A). The achieved deformation of DEAs is strongly affected by any applied mechanical loads [8]. Although large deformations have been demonstrated for DEAs under equal-bi-axial forces, only small deformations have been observed under uni-axial forces. In order to favor large uni-axial deformations, it is predicted that DEAs ought to be pre-stretched or constrained in the other direction. This can be achieved by creating uni-axial fiber reinforced DEAs (uFRDEAs). Such actuators are considered transversely isotropic, as their properties are dependent on the direction of the fibers.

This work studies the use of fiber reinforcement of DEAs to achieve large uni-axial strains. Current models for uFRDEAs found in literature [8] consider that there is no displacement in the fiber direction, simplifying the model to a uni-directional strain configuration, although the fiber constraint is found to be imperfect and dependent on the fibers chosen. The proposed model innovates by taking into consideration the fiber material, properties and dimensions, and is characterized by hyperelastic isotropic models for conventional actuators and transversely isotropic models for uFRDEAs. In the past years, several models have been proposed for hyperelastic anisotropic materials, based on strain energy functions [9]. The aim of such models is to investigate the mechanical behavior, and they are mostly developed for the characterization of soft biological tissues [10]. Some of the most popular anisotropic strain energy functions include the Fung-type model [11, 12] with an exponential form, which inspired a lot of work for the understanding and modeling of soft tissues [13]. It is also common to separate the energy density function into an isotropic and an anisotropic parts, corresponding to the matrix and to the behavior of the fibers respectively. Among such models, the HGO model proposed by Holzapfel *et al* [14] can be cited, which has also been extended to take into account the distribution and the fiber-matrix interactions [15].

Once the model of the actuators is established, a novel fabrication process for reinforcing DEAs is proposed by embedding 3D printed fibers fabricated by fused deposition modeling and tuning the infill of the part. Currently, fiber reinforced actuators found in literature are fabricated by sandwiching the fibers between the dielectric and the electrodes, or embedding the fibers inside one of the layers. Fibers can be made of nylon [8], commercial polyethylene fibers [16], cotton coated polyester fibers [17], or carbon fiber fabric [18]. Commercially available fibers however limit the design freedom of the actuator, and sometimes can be hard to embed in a planar DEA, as alignment of the fibers can be delicate. The use of 3D printed fibers allows a fast, simple and modular fabrication of fibers.

In this work, the theory of uni-axial DEAs is established for fiber reinforced configurations. The actuators are fabricated and analyzed. The proposed model and invariant based strain energy function and the experimental data are compared over the regions of interest. Finally, the challenges and future perspectives of such uFRDEAs are discussed.

2. Modelling of the actuator

The theory and models of DEAs are established in order to study the electromechanical response of the actuators under uni-axial forces. A schematic illustrating the two actuators, at rest and when a voltage is applied, is shown on figures 1(A) and (B).

When a voltage is applied on a DEA, a compressive Maxwell stress will induce a thickness reduction. The electrostatic pressure in the thickness direction when voltage is applied can then be written as in equation (1), where V refers to the voltage applied across the DEA, l_z to the thickness of the DEA, ϵ_r and ϵ_0 denote the material relative permittivity and the absolute permittivity respectively. The true electric field of the DEA is defined as $E = \frac{V}{l_z}$

$$p = -\frac{\epsilon_0 \epsilon_r V^2}{l_z^2} = -\epsilon E^2 \tag{1}$$

The theory of DEAs has been reviewed by Suo [19]. In this paper, the main ideas relevant to uni-axial deformations will be taken into consideration, for DEAs subject to external mechanical loading in the y-direction as in figures 1(A) and (B).

The nominal stresses in each direction are denoted by s_i (where $i = x$, y and z). The stretch ratio λ_i is also defined, as $\frac{l_i}{L_i}$, where l_i is the effective length and L_i is the original length. The nominal electric field can be noted $\tilde{E}$ such as $E = \lambda_x \lambda_y \tilde{E}$.

The equations of state for a DEA can be written as [19]:

$$s_i = \frac{\partial W\left(\mathbf{C}, \tilde{E}\right)}{\partial \lambda_i} \tag{2}$$

W refers to the strain energy density of the system, composed by the mechanical strain component, W_s and the electrical component, W_E, such as:

$$W\left(\mathbf{C}, \tilde{E}\right) = W_\mathrm{s}\left(\mathbf{C}\right) + W_\mathrm{E}\left(\mathbf{C}, \tilde{E}\right). \tag{3}$$

$\mathbf{C}$ refers to the Cauchy Green deformation tensor such as:

$$\mathbf{C} = \begin{bmatrix} \lambda_x^2 & 0 & 0 \\ 0 & \lambda_y^2 & 0 \\ 0 & 0 & \lambda_z^2 \end{bmatrix}. \tag{4}$$

2.1. Conventional actuator

Considering DEAs as a homogeneous, isotropic elastomeric membrane, the mechanical strain energy density can be written by adopting a free energy function for hyperelastic materials. For isotropic membranes, the strain energy function can be defined as a function of the three first invariants of the Cauchy Green tensor, namely I_1, I_2 and I_3:

$$I_1 = tr\left(\mathbf{C}\right) = \lambda_x^2 + \lambda_y^2 + \lambda_z^2 \tag{5}$$

$$I_2 = \frac{1}{2} \cdot \left[tr\left(\mathbf{C}\right)^2 - tr\left(\mathbf{C}^2\right)\right] = \lambda_x^2\lambda_y^2 + \lambda_y^2\lambda_z^2 + \lambda_x^2\lambda_z^2 \tag{6}$$

$$I_3 = det\left(\mathbf{C}\right) = \lambda_x^2\lambda_y^2\lambda_z^2. \tag{7}$$

For incompressible materials, I_3 equals to 1 as the volume is conserved—the relation (8) is then established

$$\lambda_x\lambda_y\lambda_z = 1 \Rightarrow \lambda_z = \frac{1}{\lambda_x\lambda_y}. \tag{8}$$

In this paper, the Yeoh model is used, in order to determine the strain energy density function W_s

$$W_\mathrm{s}\left(\mathbf{C}\right) = W_\mathrm{s}\left(I_1\right) = \sum_{i=3}^{3} C_{i0}\left(I_1 - 3\right)^i \tag{9}$$

where the C_{i0} parameters can be determined through an uni-axial test according to the boundary conditions [20] and are regrouped in annex.

For a uni-axial membrane along the y-direction, the principal stretch λ is defined as $\lambda = \lambda_y$. It is then possible to write the Cauchy Green deformation tensor from equation (4) as:

$$\mathbf{C} = \begin{bmatrix} \frac{1}{\lambda_y} & 0 & 0 \\ 0 & \lambda_y^2 & 0 \\ 0 & 0 & \frac{1}{\lambda_y} \end{bmatrix}. \tag{10}$$

Therefore, the first invariant is written as:

$$I_1 = \lambda_y^2 + \frac{2}{\lambda_y}. \tag{11}$$

And the strain energy density function is written as:

$$W_\mathrm{s}\left(\mathbf{C}\right) = W_\mathrm{s}\left(\lambda_y\right) = \sum_{i=3}^{3} C_{i0}\left(\lambda_y^2 + \frac{2}{\lambda_y} - 3\right)^i. \tag{12}$$

2.2. uFRDEAs

uFRDEAs are considered as transversely isotropic, with properties that are dependent on the direction of the fibers. To take into account this anisotropy, the strain energy function can be defined as a function of the three first invariants of the Cauchy Green tensor, and two additional quasi invariants [21, 22], which are based on the orientation of the fibers in the materials, by using a direction vector $\mathbf{a}_0$. The quasi invariants, I_4 and I_5 can be written as:

$$I_4 = \mathbf{a_o}\mathbf{C}\mathbf{a_o} = \lambda_\mathrm{F}^2 \tag{13}$$

$$I_5 = \mathbf{a_o}\mathbf{C}^2\mathbf{a_o} = \lambda_\mathrm{F}^4 \tag{14}$$

and the strain energy density becomes

$$W_\mathrm{s} = W_\mathrm{s}\left(I_1, I_2, I_3, I_4, I_5\right). \tag{15}$$

λ_F corresponds to the strain in the fiber direction. In the particular case of uni-axial fibers, where $\mathbf{a}_0 = [100]$ as in figure 1(B), the quasi invariants become $I_4 = \lambda_x^2$ and $I_5 = \lambda_x^4$.

The strain energy can be separated into two components: first, the energy stored in the isotropic elastomer matrix, denoted W_iso, and secondly, the energy stored in the anisotropic fiber reinforcement, W_aniso. The volume fraction of the

dielectric matrix and of the fibers are introduced as v_{M} and v_{f} respectively.

$$W_{\mathrm{s}} = v_{\mathrm{m}} \cdot W_{\mathrm{iso}}\left(I_1, I_2, I_3\right) + v_{\mathrm{f}} \cdot W_{\mathrm{aniso}}\left(I_4, I_5\right). \tag{16}$$

With $V_{\mathrm{M}} = L_x L_y L_z$. W_{iso} can be written by adopting the Yeoh model, such as:

$$W_{\mathrm{iso}}\left(I_1, I_2, I_3\right) = W_{\mathrm{iso}}\left(I_1\right) = \sum_{i=3}^{3} C_{i0}\left(I_1 - 3\right)^i \tag{17}$$

where the C_{i0} parameters can be determined through an uni-axial test according to the boundary conditions [20].

The volume ratio, v_{m} is defined such as $v_{\mathrm{m}} = \frac{V_{\mathrm{M}}}{V_{\mathrm{total}}} = \frac{V_{\mathrm{M}}}{V_{\mathrm{F}}+V_{\mathrm{M}}}$ where V_F is the volume of the fibers. Under the assumption that the fibers are a linear elastic material and thus have a linear stress/strain relationship for low strains, their Young modulus is defined as E_{f}. The fibers are considered to have a cross section area of A_{f} and an initial length L_{f}. A change in the fiber length d_x is defined for a segment d_l of a fiber. Given a force F_{f}, the linear elastic relationship is $\frac{F_{\mathrm{f}}}{A_{\mathrm{f}}} = \epsilon_{\mathrm{f}} E_{\mathrm{f}}$, where $\epsilon_{\mathrm{f}} = \mathrm{d}x/\mathrm{d}l$.

The strain energy stored in the segment d_{l} during the fibers' deformation, dW_{f}, is equal to the area under the force-displacement curve, and is written as:

$$\mathrm{d}W_{\mathrm{f}} = \frac{1}{2} F_{\mathrm{f}} \mathrm{d}x = \frac{1}{2} \epsilon_{\mathrm{f}} E_{\mathrm{f}} A_{\mathrm{f}} \mathrm{d}x = \frac{1}{2} {\epsilon_{\mathrm{f}}}^2 E_{\mathrm{f}} A_{\mathrm{f}} \mathrm{d}l. \tag{18}$$

By integrating equation (18), the total strain energy density of the fibers is:

$$W_{\mathrm{f}}\left(\epsilon_{\mathrm{f}}\right) = \int_0^{L_{\mathrm{f}}} \frac{1}{2} \epsilon_{\mathrm{f}} E_{\mathrm{f}} A_{\mathrm{f}} \mathrm{d}l = \frac{1}{2} \epsilon_{\mathrm{f}} E_{\mathrm{f}} A_{\mathrm{f}} L_{\mathrm{f}}. \tag{19}$$

In order to obtain W_{aniso}, the fiber strain energy density is divided by the total volume of the fibers, $V_{\mathrm{F}} = A_{\mathrm{f}} L_{\mathrm{f}} n_{\mathrm{f}}$ where n_{f} is the total number of fibers. Finally, the quasi invariant I_4 is introduced in the expression, such as $I_4 = (\epsilon_{\mathrm{f}} + 1)^2$

$$W_{\mathrm{aniso}}\left(I_4, I_5\right) = W_{\mathrm{aniso}}\left(I_4\right) = \frac{\left(\sqrt{I_4} - 1\right)^2 \cdot E_{\mathrm{f}}}{2}. \tag{20}$$

In order to take into account the effect of the fibers in the load direction, resulting from the increased rigidity of the fiber reinforced actuator, a penalty is introduced for the surface covered by the fibers, by considering that the surface underneath the fibers is not active when an electric field is applied.

For a uni-axial actuator, the Yeoh model as well as equation (1), the nominal stresses s_x and s_y can be written as in equations (21) and (22). The two equations are solved for both conventional DEAs (in which case W_{s} is defined as W_{iso}) and uFRDEAs, in which case W_{s} is defined as in equation (16)

$$s_y = \frac{F}{L_z L_y} = \frac{\partial W_{\mathrm{s}}\left(\lambda_x, \lambda_y, \tilde{E}\right)}{\partial \lambda_y} - \frac{\partial W_{\mathrm{E}}\left(\lambda_x, \lambda_y, \tilde{E}\right)}{\partial \lambda_y} \tag{21}$$

$$s_x = 0 = \frac{\partial W_{\mathrm{s}}\left(\lambda_x, \lambda_y, \tilde{E}\right)}{\partial \lambda_x} - \frac{\partial W_{\mathrm{E}}\left(\lambda_x, \lambda_y, \tilde{E}\right)}{\partial \lambda_x}. \tag{22}$$

It can be noted that for incompressible materials, I_3 equals to 1 as the volume is conserved—the relation (23) is then established

$$\lambda_x \lambda_y \lambda_z = 1 \Rightarrow \lambda_z = \frac{1}{\lambda_x \lambda_y}. \tag{23}$$

The resulting strain energy density W_{E} can then be written as:

$$W_E\left(\lambda_x, \lambda_y, \tilde{E}\right) = -\frac{\epsilon_0 \epsilon_r}{2} \tilde{E}^2 \left(\lambda_x \lambda_y\right)^2. \tag{24}$$

These two equations with two unknowns, λ_x and λ_y are solved using MATLAB (R2021a, The MathWorks, Inc. Natick, Massachusetts, USA). The results are plotted in figures 2(A) and (B), for conventional and uFRDEAs, for actuators with a dielectric layer thickness of 100 μm and a 20 mm width. The model takes into account arbitrary fiber dimensions (0.1 mm^2 cross section area and a total of ten aligned fibers) as well as an arbitrary applied load of 0.6 N in the y-direction.

It can be noted that the initial strain due to the mechanical loading is predicted to be higher for a reinforced actuator, reaching 29%, than for a conventional actuator, which reaches an initial strain of 22% in the vertical y-direction.

In the direction of the fibers, the initial strain is null for uFRDEAs, whereas the strain for conventional actuators is as expected negative and reaches a value of −9%.

For visualisation purposes, the initial strain for each configuration respectively is subtracted for the graphs. As expected, it is seen that the actuation strain in the y-direction, perpendicular to the fiber direction, is enhanced for uFRDEAs. The strain in the fiber direction (x-direction) is close to zero for uFRDEAs, proving that the fibers almost fully constraint the DEA displacement in their direction.

The cross-section area, the DEA surface covered by the fibers and the mechanical properties such as the Young's modulus of the fiber material (as regrouped in annex) can be tuned in the model and studied to evaluate the influence of each parameter and optimize the actuator performance.

A plot when varying the surface of the actuator which is covered by fibers is shown in figure 2(C).

It can be noted that the strain in the load direction increases for a larger surface covered by fibers, as more fibers allow to better constraint the movement in the fiber direction and thus increase the strain in the perpendicular direction. However, for extreme cases (coverage >60%), the resulting strain is reduced. No strain is predicted for 100% surface coverage by fibers, which is intuitive as the actuator would be too constrained.

The fiber material influences the strain in the direction of the fibers, for a predicted strain at breakdown as low as 0.07% for PLA fibers. However, the strain difference in the y-direction is not noticeable for different materials (figure 2(E)). When zooming into the model graphs a smaller difference is noticed, and the strain is from highest to lowest with a highest strain for PETG, followed by Nylon, ABS and finally PLA fibers, as seen in figure 2(F), which is directly linked to their stiffness.

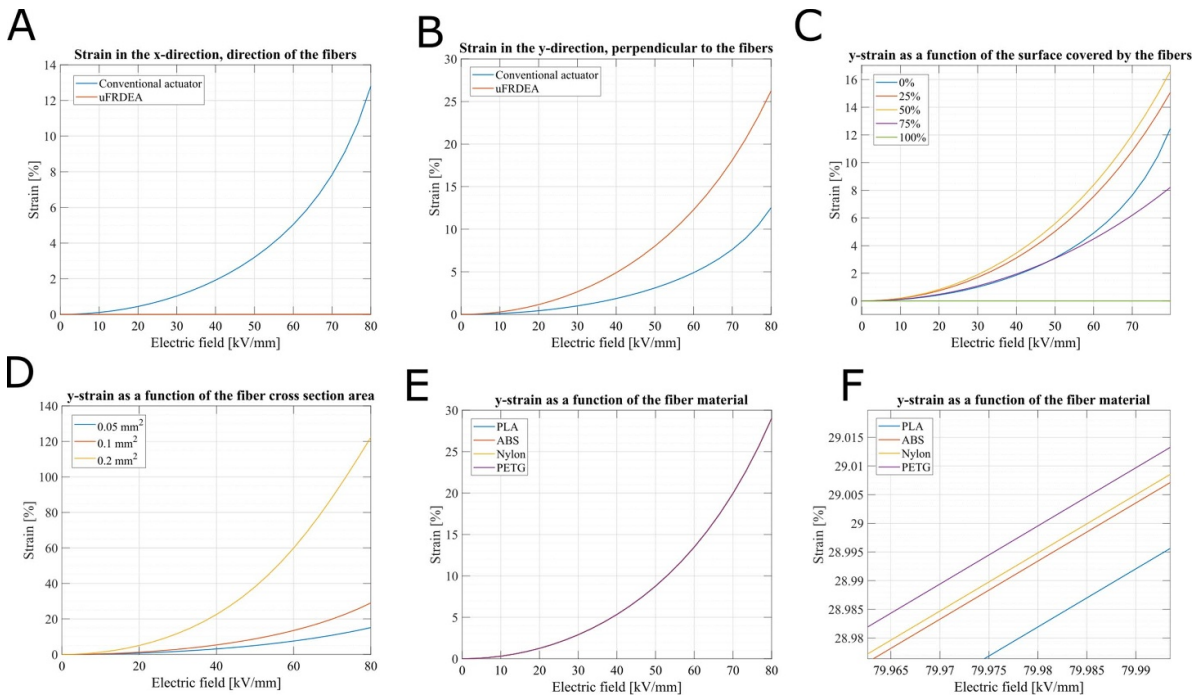

Figure 2. Model behaviour, showing the resulting strain as a function of the applied electric field; (A) in the *x*-direction. (B) in the *y*-direction. (C) in the *y*-direction, when varying the surface coverage of the fibers. (D) in the *y*-direction, when varying the fibers' cross section area. (E) in the *y*-direction, when varying the fiber material and (F) in the *y*-direction when varying the fiber material, zoomed near the breakdown field.

Lastly, in order to study the influence of the cross section area of the fiber, the surface covered by fibers, equal to the number of fibers multiplied by their width, is kept constant. The fiber cross section is modified by varying their thickness, and number of fibers to fiber width ratio. It can then be observed that the larger the cross section of the fibers, the lesser the strain in the fiber direction and greater the strain in the direction normal to the fibers as in figure 2(D).

3. Fabrication and characterization

In this study, a novel fabrication process is proposed for uFRDEAs by using the 3D printing infill method for the reinforcement of DEAs. 3D printing allows to control the exterior all as well as the infill of a part, including the infill density and infill pattern. The infill can thus be programmed to consist of aligned fibers, which would thus have a rectangular cross section. For each fiber material, the fabrication approach is similar and is illustrated in figure 3(A).

3.1. DEA fabrication

The electrodes are carbon based and the dielectric layer consists of a commercially available Elastosil ® silicone dielectric film from Wacker Chemie. First, the electrode mixture is prepared using carbon black EC-600J, isopropanol and LSR 4305 silicone. A mask for the electrode is then laser cut into a rectangular shape.

The electrode mixture is stencil printed on the Elastosil film and thermally cured at 80 °C for 4 h. In order to apply the electrode on the other side of the Elastosil, the silicone film is transferred on a new PET substrate with the electrode facing down. To that end, a silicone glue (LSR 4305) layer is applied on the first electrode while protecting a small surface in order to have access to the electrodes and thus later implement the connectors of the DEA. Finally, the second electrode is stencil printed on the other side of the Elastosil film and thermally cured in the same conditions as for the first electrode [23].

3.2. Fiber reinforcement

Fused deposition modeling (FDM) 3D printing was performed using acrylonitrile butadiene styrene (ABS orange, Flash Forge), polylactic acid (PLA lime green, Prusa research Czech Republic), polyethylene terephthalate glycol (PETG transparent, Purefil, Fabru GmbH) and nylon (FX 256, Fillamentum Manufacturing, Czech Republic). Filaments in 1.75 mm diameter were purchased and used as delivered. A Prusa MK3S+ FDM printer was used for printing all materials. A rectangular model was created in Fusion 360. The model was imported into Prusa slicer software as an .stl file and a 0.1 mm layer thickness was used for slicing. The fibers are fabricated by using the infill method. 3D printing allows to control the exterior all as well as the infill of a part, including the infill density and infill pattern. The infill can thus be programmed to consist of aligned fibers, which would thus have a rectangular cross section. Some settings (detailed in annex) were modified to ensure successful incorporation of desired infill pattern into the model.

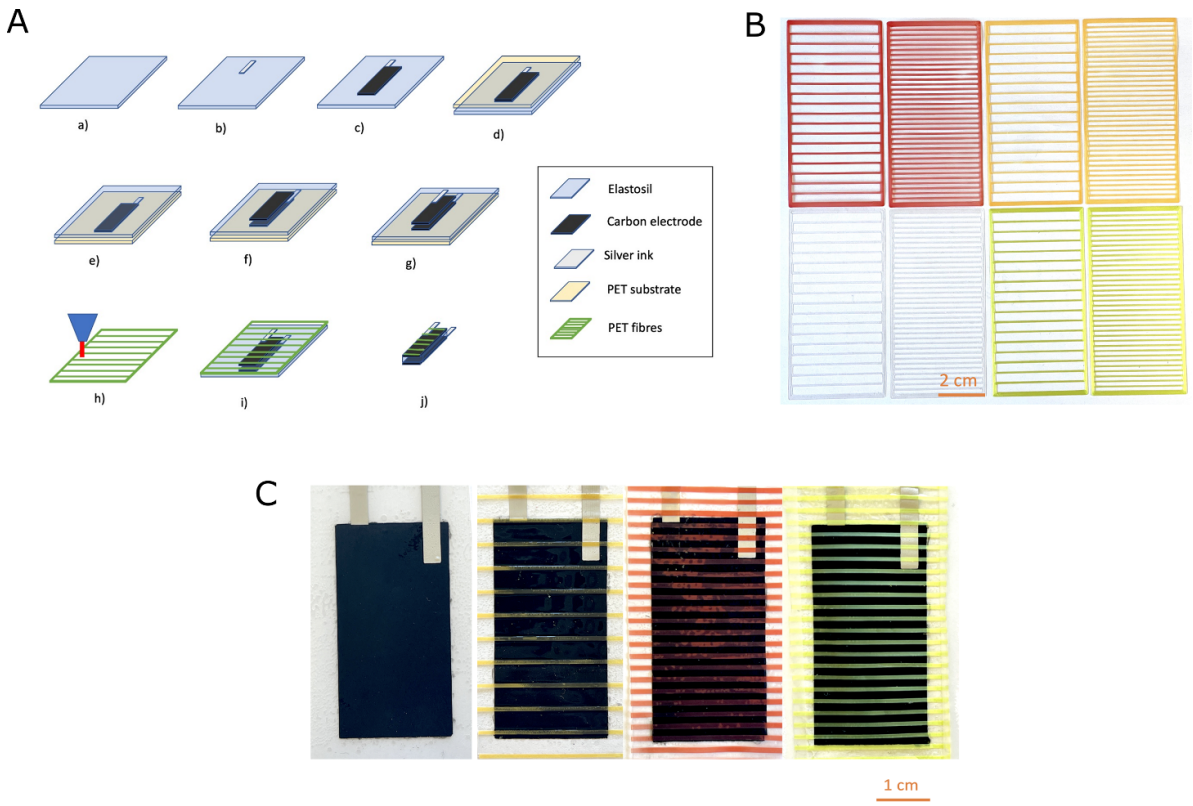

Figure 3. (A) uFRDEAs detailed fabrication process. (a) Elastosil film. (b) Stencil printing of silver ink for the connectors of the DEA. (c) Stencil printing of the first electrode. (d) Gluing of a PET substrate on top of the first electrode. (e) Flipping of the elastosil film in order to have access to the other side of the elastosil film. (f) Stencil printing of the second carbon electrode (g) Stencil printing of silver ink for the second connector. (h) Fabrication of the layer sheet into the desired fiber shape. (i) Gluing of the fibers onto the DEA and silicone encapsulation application. (j) Removing of the PET substrate and resulting DEA. (B) Examples of fabricated fiber layers, for 10% and 20% infills. From top to bottom, left to right: nylon (red), ABS (orange), PETG (transparent) and PLA (lime green). (C) Examples of fabricated DEAs. From left to right, conventional DEA without fibers, ABS fibers with 10% infill, nylon fibers with 20% infill and PLA fibers with 20% infill.

Table 1. Fiber cross section for the different materials.

	Height (μm)	Width (μm)	Cross section (mm^2)
Nylon	90	850	0.077
ABS	113	660	0.075
PETG	108	810	0.088
PLA	88	760	0.067
Mean	99.75	770	0.077

The resulting fiber layers are shown in figure 3(B). Different filament colors were used for different materials: nylon was printed with a red filament, ABS with an orange one, PETG with a transparent and finally PLA with a green lime filament. The steps corresponding to the fiber embedment in the DEA are described in figure 3(A) with step (h) illustrating the fabrication of the fibers into the desired shape, and step (i) illustrating the application of the fiber sheet onto the DEA. A frame is left around the fibers in order to keep them aligned and make the application significantly easier. The fibers are then glued on the electrode by first positioning them and then applying a silicone glue layer (LSR 4305), providing also an encapsulation layer to the DEA. Finally, the DEA is cut around the edges of the electrodes, leaving a 2 mm margin to avoid breakdown around the edges. The PET frame holding the fibers is thus cut and the uFRDEAs are ready to be actuated. Resulting actuators are shown in figure 3(E).

3.3. *Profile analysis*

The samples were analysed using a profile-analyzing laser microscope (Keyence, VK-X1000) and shown in figure 4. A region of interest around the silver connectors was considered in order to study the resulting fiber cross section depending to the materials.

The file for the fiber printing was the same for all the fibers, however a difference in the height and width for each fiber material is noticed and is detailled in table 1. The height is

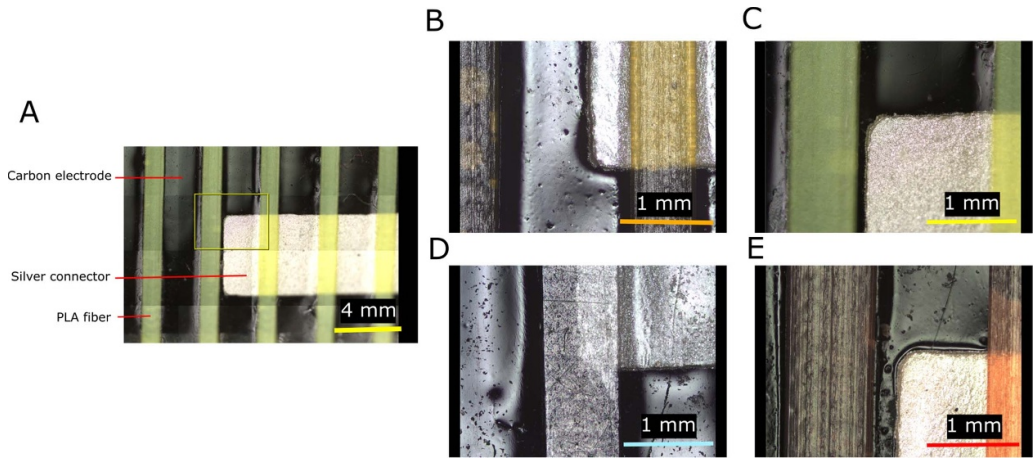

Figure 4. Imaging of the fiber reinforced actuators with the Profile-analyzing Laser Microscope. (A) Region observed, around the silver connectors and carbon electrodes. Microcope views of (B) ABS fibers. (C) PLA fibers. (D) PETG fibers. (E) Nylon fibers.

the highest for the ABS fibers and the lowest for the PLA fibers, whereas the fibers are the widest for for nylon fibers and the thinnest for the the ABS fibers. This results in a different cross section for each fiber material, with a mean of $0.077 \pm 0.011\,\text{mm}^2$.

4. Results and discussion

4.1. Validation setup

In order to study the influence of the fibers, the fabricated uFRDEAs were actuated with voltages varying from 0 to 7 kV. Two different actuators were tested for each material and four different for each number of fibers. The actuators are tested in a uni-axial load configuration as in figures 1(A) and (B). The actuators are clamped on the top side and a load is attached to the bottom side. The displacement in the load direction is measured using a laser displacement sensor (Keyence LK-G32), and the displacement in the horizontal (x-) direction is measured optically with a camera. A total number of 15 cycles was performed for each actuator. The graphs shown in figures 5(A) and 6 take into account the mean strain over all the cycles for each type of actuator. Conventional actuators with the same dimensioning were also fabricated and tested, in order to compare both the impact of the reinforcement and the fiber materials.

The proposed measurement setup matches the loading conditions illustrated in figure 1(B). The displacement in the vertical (y-) direction is measured using a laser sensor, and the displacement in the horizontal (x-) direction is measured optically with a camera.

4.2. Influence of the fibers

First, the influence of the fiber reinforcement is studied. To that end, actuators with dimensions of $2\,\text{cm} \times 4\,\text{cm} \times 100\ \mu\text{m}$ are considered: a conventional actuator and an actuator with ten PETG fibers (10% infill). The model input parameters are set accordingly and the results are shown in figure 5(A). The mean strain and its standard deviation are also plotted.

The experiments for the uFRDEAs match the model predictions with a mean error of 5% and relative standard deviation of 7%. The conventional DEAs outperform the predicted strain by 30%, which can be explained by the fact that the model considers a uniform stretch which is more accurate for the fiber reinforced configuration than for the conventional one.

Overall, the fibers allow to reach a mean strain 75% higher than the non-reinforced actuator in the load direction.

The DEA actuation is illustrated in figure 5(B). The strain in the perpendicular direction is monitored using a camera during the actuator deformation. For all fiber reinforced actuators, the strain in the fiber direction is $<1\%$, whereas for the conventional actuator, the strain reaches over 5% which is in accordance with the model predictions. Graphs of the nylon, PLA and ABS fibers' resulting strain can be found in annex. It can be noted that the response time of the actuators is improved with the use of uFRDEAs, with a decrease of up to 20% in the response time. The comparison of the step response of a uFRDEA and conventional actuator can be also be in figure 10 in annex.

4.3. Influence of the material

The resulting strain depending on the fiber material is plotted on figure 6(A). It can be noted that the model predicted a lower strain variation for the different materials in the load direction. However, a noticeable difference is measured, is the same order as it is for the model: the highest strain is noticed for PETG, followed by nylon, ABS and finally PLA fibers. The difference can be due to the different cross sections of the fibers printed. Indeed, the cross section of the PETG fibers is higher than the cross section of the PLA fibers ($0.088\,\text{mm}^2$ and $0.067\,\text{mm}^2$ respectively). According to the model in figure 2(F), a higher strain is indeed predicted for a bigger cross section.

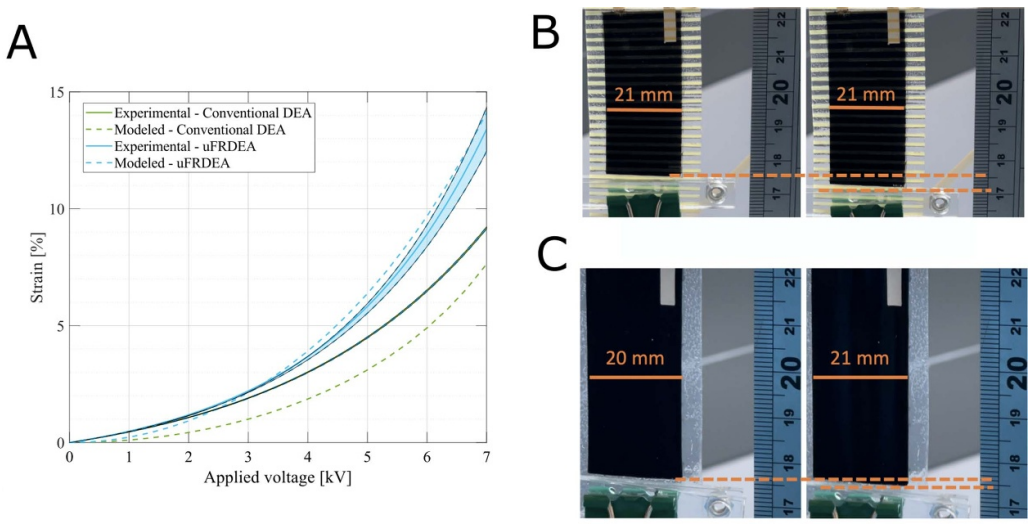

Figure 5. (A) Resulting strain for PETG fibers and their comparison to the model. An error inferior to 5% is measured between the modeled and experimental uFRDEAs. (B) Illustration of the actuation for reinforced actuators. The left panels correspond to the resting state and the right panels to the actuated state. (C) Illustration of the actuator for a conventional actuator.

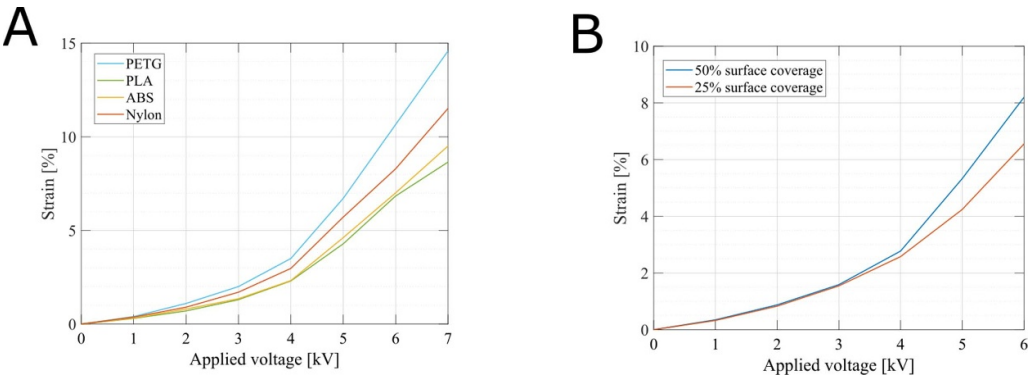

Figure 6. (A) Resulting strain for different fiber materials. (B) Resulting strain for different number of fibers, described by a different infill percentage set during printing of the fibers. 10% ans 20% printing infills correspond to a 25% and 50% actuator surface coverage, respectively.

4.4. Influence of the surface covered by the fibers

The mean resulting strain depending on the fiber infill, for all materials, is plotted on figure 6(B). As predicted by the model, the strain is higher for uFRDEAs with a higher number of fibers (resulting in a larger surface covered by fibers), independently of the fiber material. For a 10% fiber printing infill, the resulting actuator surface covered by fibers is of 25% and for 20% printing infill, it reaches 50%. It can be noted that the model predicts a strain that increases with the number of fibers up to a coverage of 60%.

From a fabrication point of view, for a higher number of fibers it was more delicate to remove the actuator from its PET substrate, which resulted in some fibers not adhering well to the DEA.

5. Conclusion

In summary, this paper focuses on enhancing the deformations of DEAs by incorporating fiber reinforcement. DEAs are materials that can produce mechanical displacement when exposed to an electric field, making them useful for applications like soft robots and haptic interfaces. However, DEAs tend to exhibit limited deformations under uni-axial forces. To overcome this limitation, the paper proposes using uFRDEAs that incorporate fibers to guide and constrain the actuator's movement along a specific direction. These fiber-reinforced actuators are characterized by their transversely isotropic properties, which means their behavior depends on the orientation of the fibers.

The paper demonstrates the potential of uFRDEAs to achieve large uni-axial strains, with a strain that is 75% higher for uFRDEAs than for traditional DEAs. The theoretical models combined with experimental validation provide insights into the electromechanical behavior of uFRDEAs. The results open up possibilities for further research to address challenges related to mechanical load effects, anisotropy, fiber alignment, scalability, and practical applications. To achieve even greater strains, it is possible to consider applying a prestretch to the actuator, in which case the model can be modified to account

for the initial forces exerted and the potential buckling of the fibers when subjected to compressive loads.

Data availability statement

The data cannot be made publicly available upon publication because no suitable repository exists for hosting data in this field of study. The data that support the findings of this study are available upon reasonable request from the authors.

Acknowledgments

This project is graciously supported by the Werner Siemens-Stiftung. The authors would also like to thank Taavet Kangur for his precious insights and help related to the 3D printing processes.

Conflict of interest

The authors declare that they have no competing interests.

Annex

Parameters of the infill method

The top and side views of the created part in figures 7(A) and (B), along with the slicer setting that were modified to ensure successful incorporation of desired infill pattern into the model are regrouped in figures 7(C) and (D).

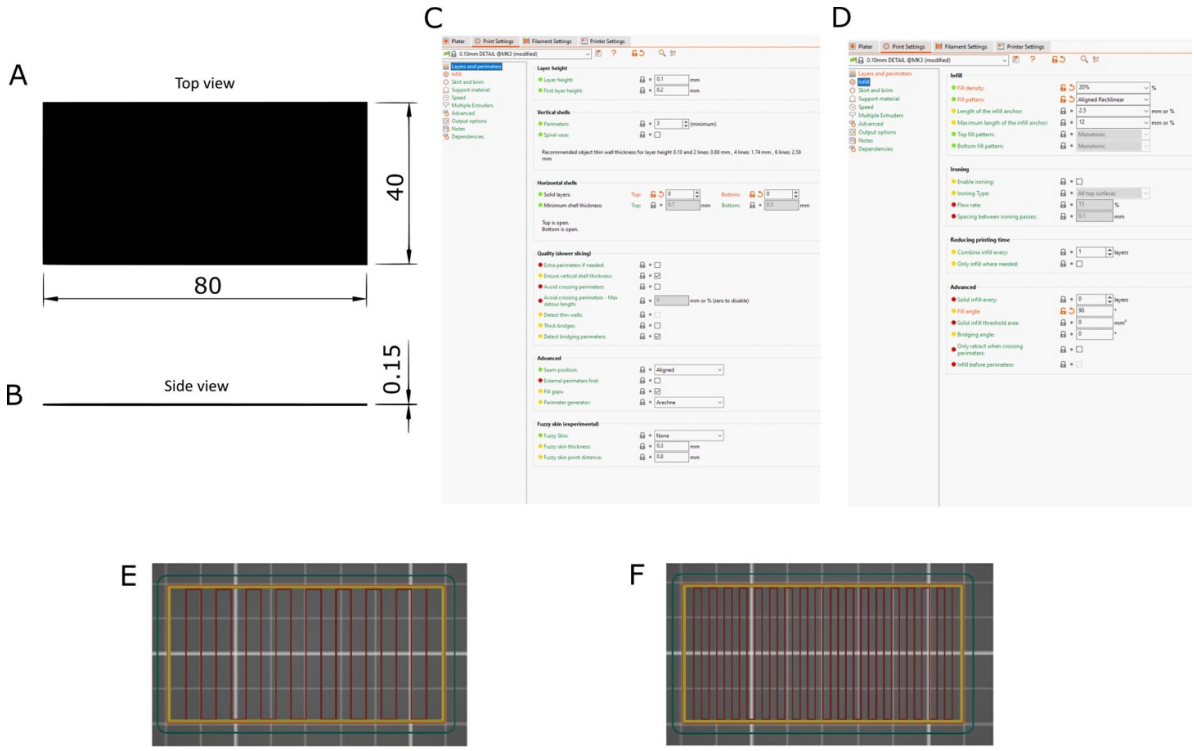

Figure 7. (A) Top view of the rectangular model created with Autodesk Fusion 360. (B) Side view of the rectangular model. (C) and (D) Parameters and modified slicer setting (in orange) for the infill method, programmed for aligned fibers. (E) Sliced model for 10% infill. (F) Sliced model for 20% infill.

SEM imaging of the fibers

SEM images of the fibers before their incorporation onto the DEA matrix were performed, in order to evaluate the fiber imperfections and the influence of the direction of printing (illustrated by the white arrows in figure 8).

Experimental results and model comparison

Resulting strain for different fiber materials and their comparison with the model are illustrated in figure 9. It can be noticed that for different materials, a difference between the model and the experimental results can be noticed. Such differences can be explained by fabrication imperfections which are not being considered by the model, such as the fiber adhesion and the fiber thickness. Depending on the actuator and fiber material, a difference in the adhesion of the fibers on the actuator can be noticed, with some fibers being detached from the actuator surface and thus influencing the performance of the uFRDEA. Such fabrication differences are however harder to quantify in the model—it could be possible to count the number of fibers that are detached and remove their influence in the model (by changing the 'number of fibers'). Another difference would come from the thickness of the fibers: indeed, when applying the glue on top of the fibers, thicker fibers will result in a thicker glue layer, thus increasing the rigidity of the actuator. This could be overcome in the model by increasing the passive ratio for thicker fiber actuators.

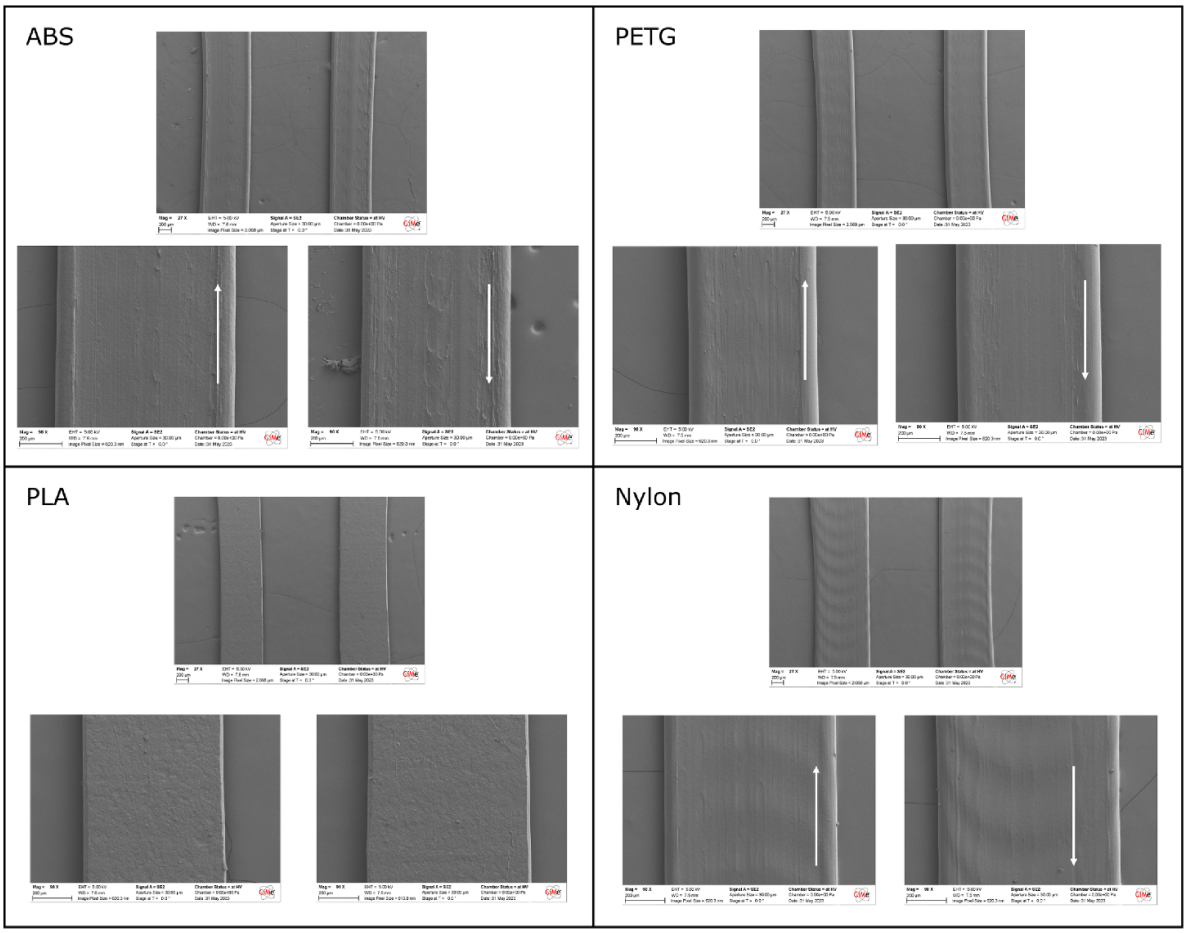

Figure 8. SEM imaging of the fibers. From top to bottom, left to right: ABS, PETG, PLA and Nylon fibers. The white arrows show the direction in which the nozzle is moving.

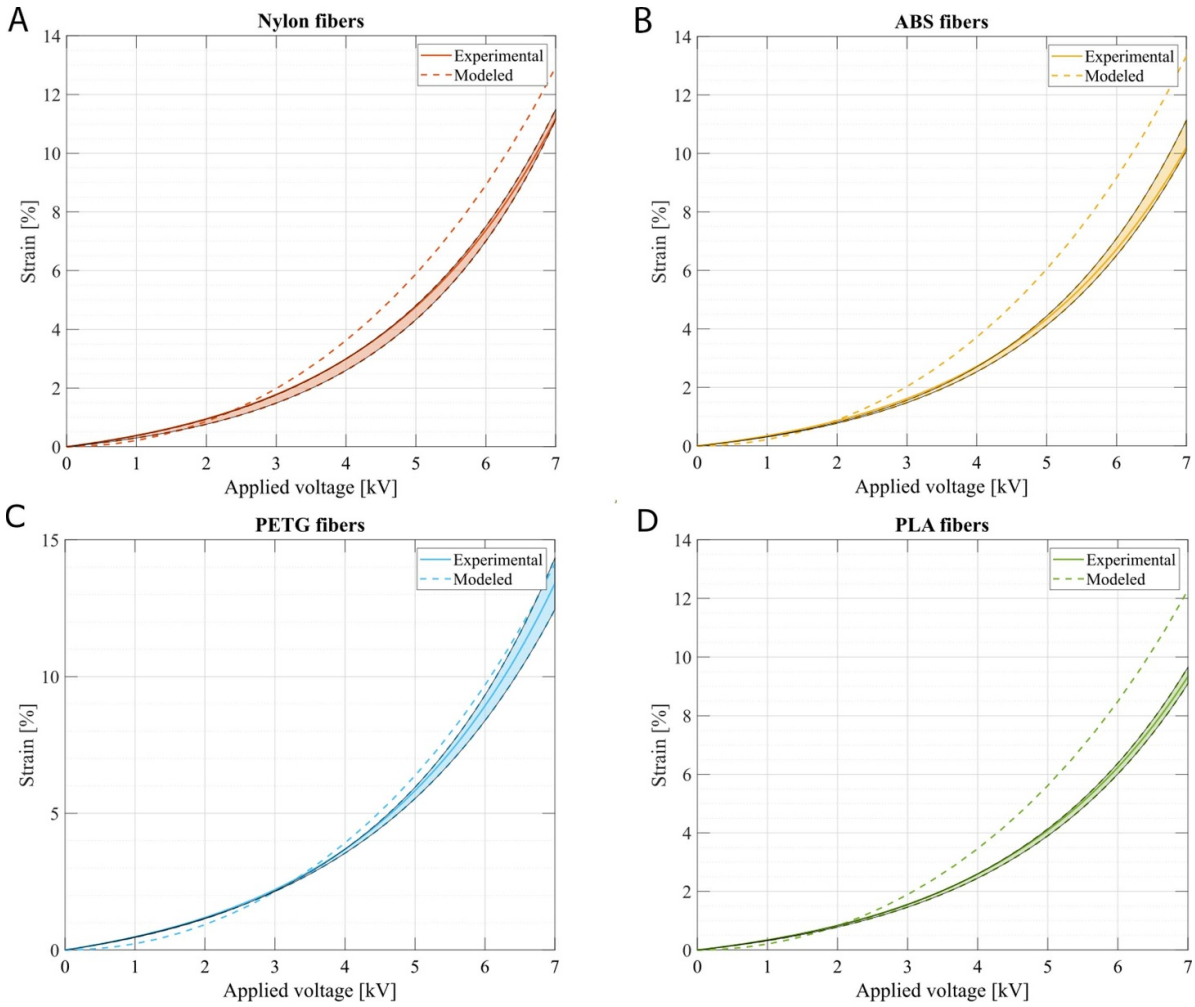

Figure 9. Resulting measured strain for different fiber materials and the corresponding predicted strain. (A) Nylon fibers. (B) ABS fibers. (C) PETG fibers. (D) PLA fibers.

Model parameters

The Ci0 parameters for the Yeoh model used are regrouped in table 2.

Table 2. Parameter values of the Yeoh model.

C10 (Pa)	C20 (Pa)	C30 (Pa)
177 620	−11 765	3894

The fiber mechanical parameters used for the model are regrouped in table 3.

Table 3. Mechanical properties for each fiber material.

Material	PLA	ABS	Nylon	PETG
Young's modulus (GPa)	1.4	2.3	2.5	3.5

Frequency response

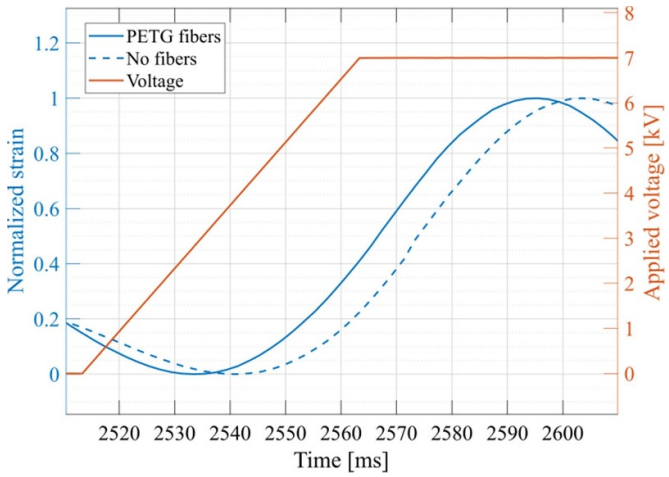

Figure 10. Step response of a uFRDEA with PETG fibers and of a conventional DEA.

ORCID iDs

Stefania Konstantinidi https://orcid.org/0000-0002-2389-4014
Thomas Martinez https://orcid.org/0000-0001-6366-1488

References

[1] Krishna S, Nagarajan T and Rani A M A 2011 *J. Appl. Sci.* **11** 1749–55
[2] Thomas S, Maquignaz G, Thabuis A and Perriard Y 2021 *2021 IEEE/RSJ Int. Conf. on Intelligent Robots and Systems (IROS)* pp 8211–6
[3] Zhang J, Sheng J, O'Neill C, Walsh C, Wood R, Ryu J-H, Desai J and Yip M 2019 *IEEE Trans. Robot.* **35** 7611
[4] Gaiser I, Schulz S, Breitwieser H and Bretthauer G 2011 *2010 IEEE Int. Conf. on Robotics and Biomimetics (ROBIO 2010)* pp 1423–8
[5] Liu L, Zhang C, Meng L, Chen X, Li D and Chen H 2017 *Smart Mater. Struct.* **26** 085018
[6] Liu W and Rahn C 2003 *J. Appl. Mech.* **70** 853
[7] Bar-Cohen Y 2002 *J. Spacecr. Rockets* **39** 822
[8] Lu T, Huang J, Jordi C, Kovacs G, Huang R, Clarke D and Suo Z 2012 *Soft Matter* **8** 6167
[9] Cai R 2017 Original strain energy density functions for modeling of anisotropic soft biological tissue *PhD Thesis* (Univ. Bourgogne Franche-Comté, UTBM)
[10] Guo Z, Shi X, Peng X and Caner F 2012 *J. Mech. Behav. Biomed. Mater.* **5** 193
[11] Fung Y 1967 *Am. J. Physiol.-Legacy Content* **213** 1532–44
[12] Fung Y 1972 *Biomechanics: Its Foundations and Objectives* (Prentice-Hall)
[13] Bhat S K and Yamada H 2021 *J. Mech. Behav. Biomed. Mater.* **125** 104959
[14] Holzapfel G, Gasser T and Ogden R 2012 *J. Elast.* **61** 1
[15] Gasser T, Ogden R and Holzapfel G 2006 *J. R. Soc. Interface* **3** 15
[16] Lee K and Tawfick S 2016 *Extreme Mech. Lett.* **8** 64–69
[17] Moss A, Krieg M and Mohseni K 2021 *IEEE Robot. Autom. Lett.* **6** 1264–71
[18] Koenigsdorff M, Mersch J, Pfeil S and Gerlach G 2022 *Proc. SPIE* **12042** 120420G
[19] Suo Z 2010 *Acta Mech. Solida Sin.* **23** 549–78
[20] Chavanne J A J-M 2019 Cylindrical dielectric elastomer actuator for cardiac assist device *Theses* EPFL, Lausanne p 168
[21] Brown L and Smith L 2011 *J. Eng. Mater. Technol.* **133** 021021
[22] Weiss J, Maker B and Govindjee S 1996 *Comput. Methods Appl. Mech. Eng.* **135** 108
[23] Martinez T *et al* 2022 *Bioeng. Transl. Med.* **8** e10396